ISSN 1674-1056
http://cpb.iphy.ac.cn
http://iopscience.iop.org/cpb
中国物理 B
Chinese Physics
中国物理 Chinese Physics B

Reconstruction of vector static magnetic field by different axial NV centers using continuous wave optically detected magnetic resonance in diamond

Jian-Feng Ye(叶剑锋), Zheng Jiao(焦铮), Kun Ma(马堃), Zhi-Yong Huang(黄志永), Hai-Jiang Lv(吕海江), Feng-Jian Jiang(蒋峰建)

Citation: Chin. Phys. B . 2019, 28(4): 047601. **doi:** 10.1088/1674-1056/28/4/047601
Journal homepage: http://cpb.iphy.ac.cn; http://iopscience.iop.org/cpb

What follows is a list of articles you may be interested in

Estimation of vector static magnetic field by a nitrogen-vacancy center with a single first-shell ^{13}C nuclear (NV-^{13}C) spin in diamond

Feng-Jian Jiang(蒋峰建), Jian-Feng Ye(叶剑锋), Zheng Jiao(焦铮), Zhi-Yong Huang(黄志永), Hai-Jiang Lv(吕海江)
Chin. Phys. B . 2018, 27(5): 057601. **doi:** 10.1088/1674-1056/27/5/057601

Experimental investigation of vector static magnetic field detection using an NV center with a single first-shell ^{13}C nuclear spin in diamond

Feng-Jian Jiang(蒋峰建), Jian-Feng Ye(叶剑锋), Zheng Jiao(焦铮), Jun Jiang(蒋军), Kun Ma(马堃), Xin-Hu Yan(闫新虎), Hai-Jiang Lv(吕海江)
Chin. Phys. B . 2018, 27(5): 057602. **doi:** 10.1088/1674-1056/27/5/057602

Large tunable FMR frequency shift by magnetoelectric coupling in oblique-sputtered $Fe_{52.5}Co_{22.5}B_{25.0}$/PZN-PT multiferroic heterostructure

Zhi-Peng Shi(时志鹏), Xiao-Min Liu(刘晓敏), Shan-Dong Li(李山东)
Chin. Phys. B . 2017, 26(9): 097601. **doi:** 10.1088/1674-1056/26/9/097601

High contrast atomic magnetometer based on coherent population trapping

Yang Ai-Lin, Yang Guo-Qing, Xu Yun-Fei, Lin Qiang
Chin. Phys. B . 2014, 23(2): 027601. **doi:** 10.1088/1674-1056/23/2/027601

Reconstruction of vector static magnetic field by different axial NV centers using continuous wave optically detected magnetic resonance in diamond*

Jian-Feng Ye(叶剑锋), Zheng Jiao(焦铮), Kun Ma(马堃), Zhi-Yong Huang(黄志永), Hai-Jiang Lv(吕海江)†, and Feng-Jian Jiang(蒋峰建)‡

School of Information Engineering, Huangshan University, Huangshan 245041, *China*

(Received 27 December 2018; revised manuscript received 25 February 2019; published online 5 March 2019)

We carried out a proof-of-principle demonstration of the reconstruction of a static vector magnetic field involving adjacent three nitrogen-vacancy (NV) sensors with corresponding different NV symmetry axes in a bulk diamond. By means of optical detection of the magnetic resonance (ODMR) techniques, our experiment employs the continuous wave (CW) to monitor resonance frequencies and it extracts the information of the detected field strength and polar angles with respect to each NV frame of reference. Finally, the detected magnetic field relative to a fixed laboratory reference frame was reconstructed from the information acquired by the multi-NV sensor.

Keywords: diamond defect, optical detection, magnetic resonance, magnetometer

PACS: 76.70.Hb, 76.30.Mi, 07.55.Ge **DOI:** 10.1088/1674-1056/28/4/047601

1. Introduction

The evaluation of a weak magnetic field with high spatial resolution has many potential applications, ranging from material science to biomedical science.[1–5] Consequently, a variety of magnetometers based on the techniques such as superconduction quantum interference devices (SQUIDs)[6] or Hall effect in semiconductors[7] have been developed in the past few decades. Alternatively, electronic spin associated with nitrogen–vacancy (NV) color center in diamond can be well addressed, initialized and manipulated, even at ambient temperature. Due to its small size and long coherence time, of milliseconds,[8] the NV center has been demonstrated to be an excellent solid-state quantum sensor that is able to detect magnetic fields with nanoscale resolution and high sensitivity.[8–22] To extract the information of detected magnetic field, the idea behind the use of NV electron is that the Zeeman shift of the electron spin sublevels is monitored through ODMR spectrums or a measurement is taken based on a quantum phase evolution.[9,10,23,24] However, due to the C_{3v} symmetry of the defect, a single NV electron spin as a magnetometer can only determine the polar angle relative to NV axis and the strength B of detected static magnetic field.[10] To reconstruct the complete information of a static vector magnetic field $\boldsymbol{B}$, the azimuth angle should be determined simultaneously. Various methods have been developed to address this issue, including the high-spin system theoretically,[25] the NV center with a single nearest neighbor ^{13}C system,[26,27] and the techniques of ensemble imaging.[28,29]

In our work, we demonstrated a proof-of-principle experiment to reconstruct a static vector magnetic field by three NV sensing spin centers with different crystal axes. By observing their respective continuous wave (CW) spectrums, we were able to reconstruct the complete information of a detected static vector magnetic field.

2. The Hamiltonian of an NV center under an applied magnetic field in diamond

The negatively charged NV center consists of a vacancy defect and an adjacent substitutional nitrogen atom. The corresponding ground state of the NV center is a spin $S = 1$ system with a zero field splitting at 2.87 GHz, separated by the lower-energy $m_s = 0$ level and $m_s = \pm 1$ levels. An external magnetic field can be applied to lift the degeneracy between the $m_S = \pm 1$ levels, as shown in Fig. 1.

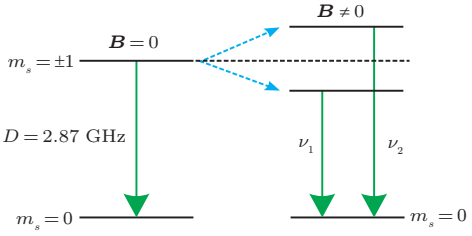


Fig. 1. The energy level scheme of NV electron spin ground states. The zero-field splitting value is $D = 2.87$ GHz. For $B \neq 0$ the split-energy levels of $m_s = \pm 1$ correspond to doublet resonance frequencies ν_1 and ν_2, respectively.

*Project supported by the National Natural Science Foundation of China (Grant Nos. 11305074, 11135002, 11804112, and 11275083), the Key Program of the Education Department Outstanding Youth Foundation of Anhui Province, China (Grant No. gxyqZD2017080), the Natural Science Foundation of Anhui Province, China (Grant No. KJHS2015B09), the Open Fund of Anhui Ley Laboratory for Condensed Matter Physics under Extreme Conditions and CAS Key Laboratory of Microscale Magnetic Resonance (Grant No. KLMMR201804), and the Fund of Scientific Research Platform of Huangshan University.

†Corresponding author. E-mail: luhj9404@mail.ustc.edu.cn

‡Corresponding author. E-mail: jfjiang@mail.ustc.edu.cn

© 2019 Chinese Physical Society and IOP Publishing Ltd

The corresponding Hamiltonian of the ground state is

$$\begin{aligned} H &= DS_z^2 + \gamma_e \boldsymbol{B}\cdot\boldsymbol{S} \\ &= DS_z^2 + \gamma_e B(\sin\theta\cos\varphi S_x + \sin\theta\sin\varphi S_y + \cos\theta S_z), \end{aligned} \quad (1)$$

where $D = 2.87$ GHz denotes the zero-field splitting, θ and φ are the polar and azimuth angles of vector magnetic field $\boldsymbol{B}$ relative to z' and x' axes in the NV frame of the reference, as shown in Fig. 5. The electron spin gyromagnetic ratio $\gamma_e = 2.8\,\text{MHz}\cdot\text{Gs}^{-1}$ ($1\,\text{Gs} = 10^{-4}$ T). The measured two resonance frequencies ν_1 and ν_2 of transitions $|m_s = 0\rangle \leftrightarrow |m_s = +1\rangle$ and $|m_s = 0\rangle \leftrightarrow |m_s = -1\rangle$ can be observed by ODMR spectrums. Correspondingly, the analytic forms of ν_1 and ν_2 are expressed as

$$\begin{aligned} \nu_1 &= \frac{2\sqrt{N}}{\sqrt{3}}\sin\left(\frac{\Omega}{3}\right), \\ \nu_2 &= \sqrt{N}\cos\left(\frac{\Omega}{3}\right) + \frac{\sqrt{N}}{\sqrt{3}}\sin\left(\frac{\Omega}{3}\right), \end{aligned} \quad (2)$$

where $\cos\Omega = M/\sqrt{M^2+K^2} = M/2\sqrt{N^3}$ and $\sin\Omega = K/\sqrt{M^2+K^2} = K/2\sqrt{N^3}$ with $M = -9(||\boldsymbol{B}||^2 - 3B_z^2)\gamma_e^2 D - 2D^3$, $N = 3||\boldsymbol{B}||^2\gamma_e^2 + D^2$, and $K = -\mathrm{i}\sqrt{-4N^3 + M^2} \geq 0$. Obviously, the two resonance frequencies $\nu_{1,2}$ depend on the magnetic field strength and vector direction relative to the NV axis.

3. Experimental setup and results

A 532-nm green laser was used for the initialization and readout of the electronic spin state. The fluorescence signal was detected by an avalanche photo diode. Coherent control of the electron spin was realized through the resonant microwave pulse radiated from a 50-μm copper line mounted on the diamond. Three different axial NV centers could be addressed using scanning confocal microscopy at room temperature.

The distance between each chosen NV center is less than 10 μm, as shown in Fig. 2. By measuring the corresponding ODMR frequencies of the NV centers with different crystallographic orientations, whose distinct CW spectrums are demonstrated under an applied static vector magnetic field, as demonstrated in Fig. 3. However, the limitation of our implementation is that the resonance frequencies measured by monitoring the CW spectrum is only applicable to detect the magnetic field strength below 0.02 T, otherwise the fluorescence of the NV center will be dramatically influenced. The resonance frequencies (shown in Table 1) could be measured by fitting experimental data. The polar angle θ and field strength B could be calculated directly from the resonance frequencies and the relative energy level shift associated with the detected field.

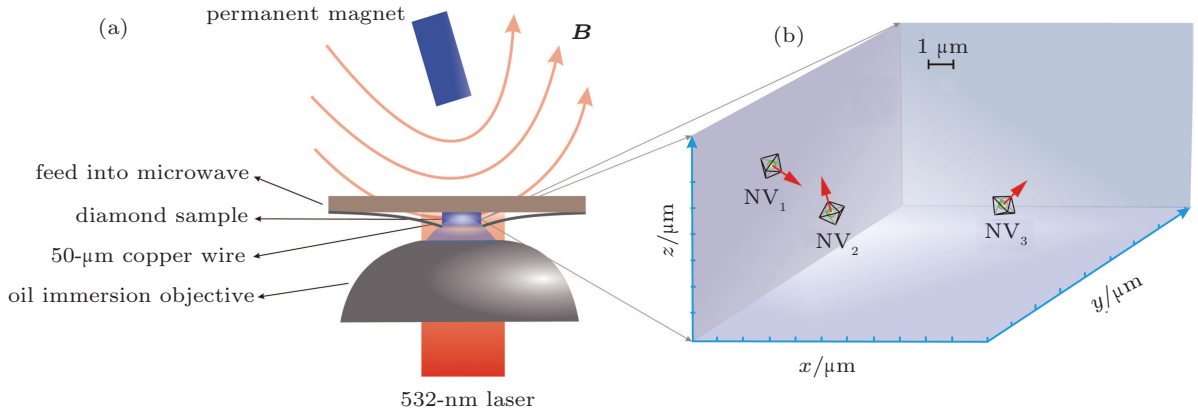


Fig. 2. A schematic diagram of the experimental setup. (a) A 532-nm laser was used for the initialization and readout of the NV electron spin. The sample was imaged with an oil immersion objective lens. (b) Zoom-in view of the diamond sample for panel (a) shows respective symmetry axes labeled by red arrows of the chosen three NV centers, the distance between them is less than 10 μm.

Table 1. Measured six resonance frequencies of CW spectrums.

Frequency	ν_1/MHz	ν_2/MHz	ν_3/MHz	ν_4/MHz	ν_5/MHz	ν_6/MHz
Experiment data	2819.7	2921.3	2836.8	2906.6	2860.6	2883.3
FWHM of CW spectra	16.7	11.6	9.9	9.7	8.0	8.2
Standard deviation	0.20	0.14	0.14	0.14	0.15	0.17

The polar angles $\theta_{1,2,3} \in [0, \pi]$ corresponding to the three NV centers could be calculated according to

$$\theta = \arccos\left(\pm\sqrt{\frac{(2\nu_1 - \nu_2 - D)(\nu_1 - 2\nu_2 + D)(\nu_1 + \nu_2 + D)}{[9D(\nu_1^2 - \nu_1\nu_2 + \nu_2^2 - D^2)]}}\right).$$

The magnetic field strength is analytically expressed by $B = \sqrt{(\nu_1^2 - \nu_1\nu_2 + \nu_2^2 - D^2)/(3\gamma_e^2)}$ (see Appendix A for details). The calculated results are listed in the following Table 2.

Table 2. The polar angles $\theta_{1,2,3}$ relative to their respective symmetry axes $\hat{e}_{\mathrm{NV}_{1,2,3}}$ and the strengths of static magnetic field B corresponding to the three NV centers.

	NV_1	NV_2	NV_3
$\theta_{1,2,3}$/rad	$(0.55 \text{ or } \pi-0.55)\pm0.03$	$(1.01 \text{ or } \pi-1.01)\pm0.005$	$(1.38 \text{ or } \pi-1.38)\pm0.003$
B/T	$(21.2\pm0.35)\times10^{-4}$	$(23.4\pm0.30)\times10^{-4}$	$(22.2\pm0.38)\times10^{-4}$

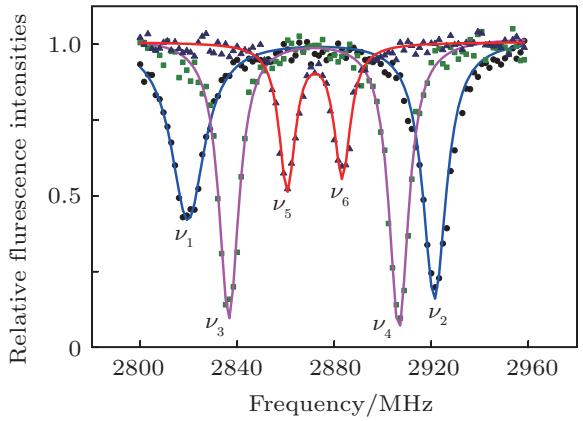


Fig. 3. Experimental data are obtained by monitoring the photoluminescence intensity. The CW spectrums of fitting curves with blue, green and red lines correspond to NV_1, NV_2, and NV_3 centers, respectively. The marked $\nu_{1,2,\ldots,6}$ correspond to their respective resonance frequencies.

4. The reconstruction of a static vector magnetic field by three different axial NV centers

To reconstruct a static vector magnetic field $\boldsymbol{B}$, the corresponding vector direction of magnetic field was projected onto Cartesian components $(\hat{x}, \hat{y}, \hat{z})$ in the laboratory frame. Alternatively, the vector field $\boldsymbol{B}$ can be projected onto each of the NV axes $\{\hat{e}_{\mathrm{NV}_1}, \hat{e}_{\mathrm{NV}_2}, \hat{e}_{\mathrm{NV}_3}, \hat{e}_{\mathrm{NV}_4}\}$ corresponds to different NV reference frames. Due to the fixed crystallographic axes inherent to the NV solid-state system, each of the tetrahedral diamond axes of NV centers demonstrates different CW spectrum features. By using a similar method as shown in Ref. [32] that reconstructed an AC vector magnetic field, a static vector magnetic field could be entirely determined by at least three of four possible NV axes aligned along $[111]$, $[\bar{1}11]$, $[1\bar{1}1]$, and $[11\bar{1}]$.

Concretely, by using a geometric arguments to transform the tetrahedral components $(\hat{x}', \hat{y}', \hat{z}')$ into a Cartesian coordinate $(\hat{x}, \hat{y}, \hat{z})$ (see Appendix B), as shown schematically in Fig. 4, the transformation between the two sets of coordinate system is given by

$$\begin{pmatrix}\cos\theta_1\\ \cos\theta_2\\ \cos\theta_3\\ \cos\theta_4\end{pmatrix} = \begin{pmatrix}0 & -\sqrt{2/3} & \sqrt{1/3}\\ -\sqrt{2/3} & 0 & -\sqrt{1/3}\\ \sqrt{2/3} & 0 & -\sqrt{1/3}\\ 0 & \sqrt{2/3} & \sqrt{1/3}\end{pmatrix}\begin{pmatrix}\sin\alpha\cos\beta\\ \sin\alpha\sin\beta\\ \cos\alpha\end{pmatrix}, \quad (3)$$

where the polar angles $\theta_{1,2,3,4}$ are taken with respect to four different NV axes $\hat{e}_{\mathrm{NV}_{1,2,3,4}}$, α and β are the polar and azimuth angles with respect to z and x axes in the laboratory frame. When the information of the four polar angles $\theta_{1,2,3,4}$ was extracted, the corresponding parameters (α, β) of the magnetic field orientation in the laboratory coordinate $(\hat{x}, \hat{y}, \hat{z})$ could be obtained based on Eq. (3). It should be noted that in our experiment only three of the four NV axes are used for reconstruction of $\boldsymbol{B}$ and the real direction of the detected field in the laboratory frame could not be determined due to the lack of a calibration of the magnetic field.

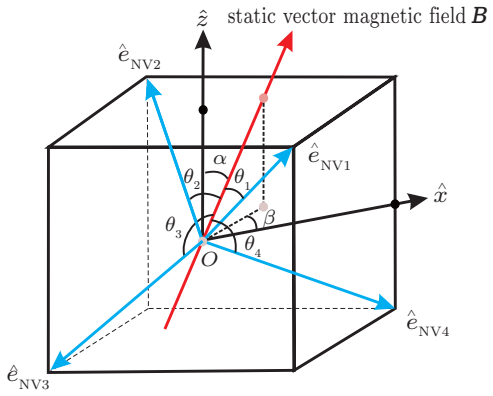


Fig. 4. Four inherent NV symmetry axes in the diamond's tetrahedral structure are demonstrated by $\hat{e}_{\mathrm{NV}_{1,2,3,4}}$. A bias static vector magnetic field $\boldsymbol{B}$ is applied. The corresponding polar angles taken with respect to each of NV axes $\hat{e}_{\mathrm{NV}_{1,2,3,4}}$ can be represented by $\theta_{1,2,3,4}$, respectively.

With a method akin to maximum likelihood estimation,[26,32] our numerical calculations implemented a search procedure to match the target experimental resonance frequencies $\nu_{1,2}$, $\nu_{3,4}$, and $\nu_{5,6}$ according to the formula

$$\Delta_{\min}(\alpha_0, \beta_0, B_0) = \min_{\alpha,\beta,B} \sqrt{[\nu_i - \nu_i'(\alpha, \beta, B)]^2}, \quad i = 1, 2, \ldots, 6, \quad (4)$$

where $\nu_i'(\alpha, \beta, B)$ denotes the searched resonance frequencies relevant to the parameters of polar angle α, azimuth angle β, and field strength B in the laboratory frame. Based on Eq. (3), one can pick up the optimal parameters α_0, β_0, and B_0 satisfying $\Delta_{\min}(\alpha_0, \beta_0, B_0)$ that minimizes Eq. (4) in comparison with other choices of parameters. In the laboratory frame, α and β relative to $\hat{z}$ and $\hat{x}$ axes and the strength of magnetic field B can be obtained, as listed in Table 3, in which the corresponding vector directions of the two results are antiparallel in the laboratory frame.

Table 3. Experimental results of detected static vector magnetic field $\boldsymbol{B}$ with respect to the laboratory frame.

	α_0/rad	β_0/rad	B_0/T	$\Delta_{\min}$/MHz
Result 1	1.34 ± 0.01	1.15 ± 0.01	$(21.1\pm0.1)\times10^{-4}$	0.68
Result 2	1.80 ± 0.01	4.29 ± 0.01	$(21.1\pm0.1)\times10^{-4}$	0.76

5. Conclusion

In this paper, we have provided an experimental study of the detection of a weak static vector magnetic field by using three NV centers with different symmetry axes under ambient conditions. By measuring the resonance frequencies of the ODMR spectrums, the corresponding information of direction and strength of the detected field could be reconstructed. In future work, it may be possible to further improve our spatial resolution by reduction of spectral broadening and determine the real vector direction of the detected magnetic field by installing the calibration of the magnetic field.

Appendix A: The determination of magnetic field strength and polar angle relative to an NV axis based on ODMR resonance frequencies

The spin Hamiltonian of the ground state of an NV center is

$$H = DS_z^2 + \gamma_e B(\sin\theta\cos\varphi S_x + \sin\theta\sin\varphi S_y + \cos\theta S_z), \quad \text{(A1)}$$

where D denotes the zero-field splitting and γ_e is the electron spin gyromagnetic ratio. The corresponding ground state eigenvalues of Eq. (A1) are given by

$$E_0 = \frac{1}{3}\left[2D - 2\sqrt{N}\times\sin\left(\frac{\Omega}{3}+\frac{\pi}{6}\right)\right], \quad \text{(A2)}$$

$$E_{-1} = \frac{1}{3}\left[2D + 2\sqrt{N}\times\sin\left(\frac{\Omega}{3}-\frac{\pi}{6}\right)\right], \quad \text{(A3)}$$

$$E_{+1} = \frac{1}{3}\left[2D + 2\sqrt{N}\times\cos\left(\frac{\Omega}{3}\right)\right], \quad \text{(A4)}$$

where $\cos\Omega = M/\sqrt{M^2+K^2} = M/2\sqrt{N^3}$, $\sin\Omega = K/\sqrt{M^2+K^2} = K/2\sqrt{N^3}$ with $M = -9(||\boldsymbol{B}||^2 - 3B_z^2)\gamma_e^2 D - 2D^3$; $N = 3||\boldsymbol{B}||^2\gamma_e^2 + D^2$; $K = -\mathrm{i}\sqrt{-4N^3+M^2}$, $K \geq 0$; $||\boldsymbol{B}||^2 = B_x^2 + B_y^2 + B_z^2$.

The corresponding two resonance frequencies are given by

$$\nu_1 = \frac{2\sqrt{N}}{\sqrt{3}}\sin\left(\frac{\Omega}{3}\right), \qquad \nu_2 = \sqrt{N}\cos\left(\frac{\Omega}{3}\right) + \frac{\sqrt{N}}{\sqrt{3}}\sin\left(\frac{\Omega}{3}\right), \quad \text{(A5)}$$

which can derive

$$||\boldsymbol{B}||^2 = \frac{(\nu_1^2 - \nu_1\nu_2 + \nu_2^2) - D^2}{3\gamma_e^2}, \qquad \theta = \arccos\left(\pm\sqrt{\frac{(2\nu_1 - \nu_2 - D)(\nu_1 - 2\nu_2 + D)(\nu_1 + \nu_2 + D)}{[9D(\nu_1^2 - \nu_1\nu_2 + \nu_2^2 - D^2)]}}\right).$$

Appendix B: The transformation between laboratory and NV frame of reference

The transformation of laboratory and NV_1 frame of reference is shown in Fig. B1. For example, the transformation between laboratory and NV_1 frame of reference is given by a 3×3 orthogonal rotation matrix

$$R_{NV_1} = \begin{pmatrix} 1 & 0 & 0 \\ 0 & \sqrt{1/3} & \sqrt{2/3} \\ 0 & -\sqrt{2/3} & \sqrt{1/3} \end{pmatrix}. \quad \text{(B1)}$$

The vector direction of $\boldsymbol{B}$ can be represented by a unit vector

$$\hat{n}_L = [\sin\alpha\cos\beta, \sin\alpha\sin\beta, \cos\alpha]^T$$

in the laboratory frame of reference.

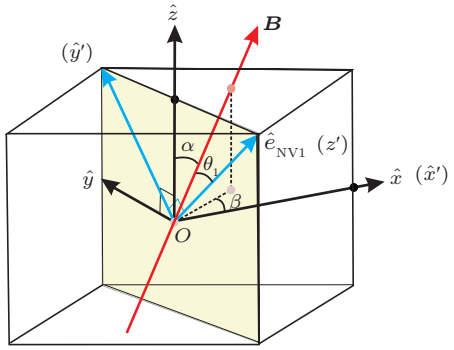


Fig. B1. The transformation of laboratory and NV_1 frame of reference are linked by a rotation around the $\hat{x}$ ($\hat{x}'$) axis. It is noted that the two reference frames share a same $\hat{x}$ axis.

Via the rotation matrix of Eq. (B1), the transformed vector direction $\hat{n}_{NV_1}$ of $\boldsymbol{B}$ in the NV_1 frame of reference can be expressed as $\hat{n}_{NV_1} = R_{NV_1}\hat{n}_L$. Due to the C_{3V} symmetry of the NV center, the main concern is the z component of $\hat{n}_{NV_1}$ parallel to the NV_1 axis $\hat{e}_{NV_1}$ as the following matrix multiplication

$$\begin{pmatrix} 1 & 0 & 0 \\ 0 & \sqrt{1/3} & \sqrt{2/3} \\ 0 & -\sqrt{2/3} & \sqrt{1/3} \end{pmatrix}\begin{pmatrix} \sin\alpha\cos\beta \\ \sin\alpha\sin\beta \\ \cos\alpha \end{pmatrix} = \begin{pmatrix} \cdots \\ \cdots \\ -\sqrt{2/3}\sin\alpha\sin\beta + \sqrt{1/3}\cos\alpha \end{pmatrix} = \begin{pmatrix} \cdots \\ \cdots \\ \cos\theta_1 \end{pmatrix}. \quad \text{(B2)}$$

In the same way, $\cos\theta_2$, $\cos\theta_3$, and $\cos\theta_4$ can be given by the transformation taken with respect to each NV reference frame.

Acknowledgments

We thank Peng-Fei Wang and Hong-Wei Chen for their helpful discussions.

References

[1] Freeman M R and Choi B C 2001 *Science* **294** 1484
[2] Budker D and Romalis M 2007 *Nat. Phys.* **3** 227
[3] Greenberg Ya S 1998 *Rev. Mod. Phys.* **70** 175
[4] Grinolds M S, Maletinsky P, Hong S, Lukin M D, Walsworth R L and Yacoby A 2011 *Nat. Phys.* **7** 687
[5] Degen C L, Reinhard F and Cappellaro P 2017 *Rev. Mod. Phys.* **89** 035002
[6] Bending S J 1999 *Adv. Phys.* **48** 449
[7] Chang A M, Hallen H D, Harriott L, Hess H F, Kao H L, Kwo J, Miller R E, Wolfe R, van der Ziel J and Chang T Y 1992 *Appl. Phys. Lett.* **61** 1974
[8] Balasubramanian G, Neumann P, Twitchen D, Markham M , Kolesov R, Mizuochi N, Isoya J, Achard J, Beck J, Tissler J, Jacques V, Hemmer P R, Jelezko F and Wrachtrup J 2009 *Nat. Mater.* **8** 383
[9] Maze J R, Stanwix P L, Hodges J S, Hong S, Taylor J M, Cappellaro P, Jiang L, Gurudev Dutt M V, Togan E, Zibrov A S, Yacoby A, Walsworth R L and Lukin M D 2008 *Nature* **455** 644
[10] Balasubramanian G, Chan I Y, Kolesov R, Al Hmoud M, Tisler J, Shin C, Kim C, Wojcik A, Hemmer P R, Krueger A, Hanke T, Leitenstorfer A, Bratschitsch R, Jelezko F and Wrachtrup J 2008 *Nature* **455** 648
[11] Chang Y R, Lee H Y, Chen K, Chang C C, Tsai D S, Fu C C, Lim T S, Tzeng Y K, Fang C Y, Han C C, Chang H C and Fann W 2008 *Nat. Nanotechnol.* **3** 284
[12] McGuinness L P, Yan Y, Stacey A, Simpson D A, Hall L T, Maclaurin D, Prawer S, Mulvaney P, Wrachtrup J, Caruso F, Scholten R E and Hollenberg L C L 2011 *Nat. Nanotechnol.* **6** 358
[13] de Lange G, Riste D, Dobrovitski V V and Hanson R 2011 *Phys. Rev. Lett.* **106** 080802
[14] Horowitz V R, Aleman B J, Christle D J, Cleland A N and Awschalom D D 2012 *Natl. Acad. Sci. USA* **109** 13493
[15] Hirose M, Aiello C D and Cappellaro P 2012 *Phys. Rev. A* **86** 062320
[16] Pham L M, Bar Gill N, Belthangady C, Le Sage D, Cappellaro P, Lukin M D, Yacoby A and Walsworth R L 2012 *Phys. Rev. B* **86** 045214
[17] Nusran N M and Dutt M V G 2013 *Phys. Rev. B* **88** 220410
[18] Loretz M, Rosskopf T and Degen C L 2013 *Phys. Rev. Lett.* **110** 017602
[19] Le Sage D, Arai K, Glenn D R, DeVience S J, Pham M L, Rahn Lee L, Lukin M D, Yacoby A, Komeili A and Walsworth R L 2013 *Nature* **496** 486
[20] Geiselmann M, Juan M L, Renger J, Say J M, Brown L J, de Abajo F J G, Koppens F and Quidant R 2013 *Nat. Nanotechnol.* **8** 175
[21] Chaudhry Adam Zaman 2014 *Phys. Rev. A* **90** 042104
[22] Chaudhry Adam Zaman 2015 *Phys. Rev. A* **91** 062111
[23] Hall L, Simpson D and Hollenberg L 2013 *MRS Bull.* **38** 162
[24] Hong S, Grinolds M S, Pham L M, Le Sage D, Luan L, Walsworth R L and Yacoby A 2013 *MRS Bull.* **38** 155
[25] Lee S Y, Niethammer M and Wrachtrup J 2015 *Phys. Rev. B* **92** 115201
[26] Jiang F J, Ye J F, Jiao Z, Jiang J, Ma K, Yan X H and Lv H J 2018 *Chin. Phys. B* **27** 057602
[27] Jiang F J, Ye J F, Jiao Z, Huang Z Y and Lv H J 2018 *Chin. Phys. B* **27** 057601
[28] Maertz B, Wijnheijmer A, Fuchs G, Nowakowski M and Awschalom D 2010 *Appl. Phys. Lett.* **96** 092504
[29] Jennifer M Schloss, John F Barry, Matthew J Turner and Ronald L Walsworth 2018 *Phys. Rev. Appl.* **10** 034044
[30] Steinert S, Dolde F, Neumann P, Aird A, Naydenov B, Balasubramanian G, Jelezko F and Wrachtrup J 2010 *Rev. Sci. Instrum.* **81** 043705
[31] Kitazawa Sayaka, Matsuzaki Yuichiro, Soya Saijo, Kakuyanagi Kosuke, Saito Shiro and Ishi-Hayase Junko 2017 *Phys. Rev. A* **96** 042115
[32] Wang P F, Yuan Z H, Huang P, Rong X, Wang M Q, Xu X K, Duan C K, Ju C Y, Shi F Z and Du J F 2015 *Nat. Commun.* **6** 6631